Theor Appl Climatol (2012) 107:297–311
DOI 10.1007/s00704-011-0461-5

ORIGINAL PAPER

Caribbean hurricanes: changes of intensity and track prediction

Mark R. Jury · Rosimar Rios-Berrios · Eduardo García

Received: 8 December 2010 / Accepted: 20 May 2011 / Published online: 9 July 2011

Abstract The meteorological conditions of hurricanes passing near Puerto Rico (18N, 68W) are analyzed using composite daily reanalysis and satellite data. When an intense hurricane is present, the regional circulation is dominated by upper easterly flow over the Caribbean and central Atlantic and a surge of low-level westerly anomalies across the tropics. Warm SST anomalies extend along the coast of Venezuela, doubling the convective energy available to Caribbean hurricanes. Intensifying hurricanes tend to propagate westward with an atmospheric ridge over the Gulf Stream, in an environment with aerosol optical depth <0.6. Hurricanes form and strengthen in the east-shear phase of the Madden Julian Oscillation. Sinking motions and dry air appear in an anti-cyclonic gyre behind intensifying hurricanes. Numerical model 48-h forecasts of Caribbean hurricane tracks are analyzed over the period 2000–2010. A "slow right" bias is found east of Puerto Rico in comparison with observed.

1 Introduction

Hurricanes have a great socioeconomic impact on the Caribbean region, extending southeastward from Key West, Florida (25N, 82W) to Barbados (12N, 58W). The risk of landfall depends on track, while the level of destruction depends on intensity, and both depend on the surrounding environmental conditions. There is a depth of knowledge on Atlantic hurricanes due to a long history of detailed observations (Landsea 1993). Much of our current knowledge is focused on USA land-falling events (Elsner et al. 1999, 2000). Less work on the behavior of hurricanes is available for the lower latitudes. The research reported here is part of an effort to better understand the interaction between Caribbean hurricanes and their surrounding environment, with a focus on changes in track and strength as influenced by sea surface temperatures (SST) and wind shear, among other factors. Emanuel (2005) and Webster et al. (2005) suggest that rising global temperatures may explain the recent upswing in the frequency and intensity of Atlantic hurricanes. Wind shear over the tropical Atlantic is an important factor determining hurricane frequency (Aiyyer and Thorncroft 2006).

Numerical models provide useful forecasts of baroclinic events; however, tropical storms remain a difficult problem (Braun 2002). Mesoscale cloud-resolving models are showing increasing skill in narrowing the across-track spread and intensity error bars for major hurricanes at multi-day lead times (McAdie and Lawrence 2000; Franklin et al. 2003; DeMaria et al. 2005). Hurricane tracks tend to split near Puerto Rico and move either north or south of the Antilles chain. Small forecast errors at the point of the track split may be compounded downstream. Pattern recognition and forecast analogs offer a way of meeting such challenges (Root et al. 2007) under the premise that weather sequences tend to repeat with similar environmental forcing in historical data sets. An analysis of cases meeting a set of criteria could provide useful guidance, if reproducible analogs emerged (Van den Dool 1994) for hurricanes in our "target" area (Kruizinga and Murphy 1983; Vislocky and Young 1989).

M. R. Jury · R. Rios-Berrios · E. García
Physics Department, University of Puerto Rico,
Mayagüez, USA

M. R. Jury (✉)
Univ. Zululand,
KwaDlangezwa, South Africa
e-mail: mark.jury@upr.edu

According to National Hurricane Center (NHC) reports, track forecast errors in the Atlantic basin have decreased 1% a year since 1980 (McAdie and Lawrence 2000). Although model performance has improved (Aberson 2001) landfall position errors have remained constant (Powell and Aberson 2001). A study by Franklin et al. (2003) confirmed that track forecast errors decreased with time, and track forecasts for marine systems were better than those for storms threatening land. As numerical models are important tools that help NHC create official track forecasts, many studies have evaluated their skill. DeMaria et al. (1989) compared track forecast errors for four different models being used at that time and found that the statistical–dynamical model produced the smallest error, whereas global baroclinic-dynamical models had the greatest error. Elsberry (1995) described how numerical models have improved in terms of environment–hurricane interactions. Goerss (2000) evaluated hurricane track predictions and found that an ensemble mean of many dynamical models reduced the forecast errors.

Here, we seek answers to three questions: what are the environmental patterns favoring the passage of hurricanes over the Antilles Islands? What induces rapid changes in hurricane intensity near Puerto Rico? How well do numerical models predict the track of hurricanes in the study area? We wish to determine if certain patterns of SST and wind shear favor an "Antilles track."

2 Data and methods

Much of this research is based on NHC HURDAT: the official hurricane reanalysis database for the Atlantic basin (Landsea CW et al. 2004). We focus on hurricanes with sustained winds (Vmax) >50 m/s with an eye passing <250 km from Puerto Rico. In the first section of our research, these criteria led us to seven cases since 1960 (Table 1). A further check was performed to find the day when the hurricane eye was closest to 18N, 67W (hereafter Day 0). Information on impacts and economic losses caused by the hurricanes were extracted from the NHC archives. Damage estimates were adjusted to "year-2000 dollars" using a 5% inflation rate to facilitate comparison. As digital IR satellite imagery is needed to quantify changes in hurricane intensity (Dvorak technique), the period after 1976 was considered for the analysis in Section 3.3. A "change index" was formulated based on the HURDAT pressure tendency scaled by wind: −(dPmin) (Vmax/Vmean); where dPmin is the change in minimum central pressure over 1 day, Vmax is the maximum sustained wind and Vmean is the Caribbean hurricane average (46 m/s) near Puerto Rico. Applying the index to all Caribbean hurricanes, the data were sorted and the top (intensify) and bottom (decay) five cases were chosen for analysis (Table 2). With cases thus identified by a narrow set of criteria, composite environmental fields were mapped using NCEP data as described below.

NCEP assimilates meteorological and physical oceanographic data since 1948 using a T62 (209 km) global spectral model with 28 vertical levels, as implemented for operational weather forecasting in the late 1990s. The vertical structure resolves tropospheric structure reasonably well, but the horizontal resolution is too coarse to resolve hurricanes. The model is continuously "nudged" with new data; otherwise, the first-guess field around the hurricane becomes too dry. Our focus on the area of Puerto Rico ensures an adequate data density. NCEP data are analyzed from the IRI Climate Library website as composites for days when hurricanes pass near Puerto Rico (Table 1). The analyzed variables, include SST, precipitable water, geopotential height, wind and its derivatives at lower and upper levels, and NOAA satellite OLR. Changes in hurricane intensity (Table 2) are analyzed by subtracting decaying from intensifying fields in the period since 1976. We perform statistical tests and focus our interpretation on composite patterns where signals exceed intra-case standard deviations.

SST is a determinant of hurricane strength (Emanuel 2005; Webster et al. 2005; Elsner et al. 2006) and has been measured around the Caribbean by ships since the late 1800s and since 1979 by satellite IR radiometers. Precipitable water is used to understand the tropospheric water vapor content surrounding hurricanes and is assimilated from radiosonde data since 1955 and from satellite since the early 1980s. The geopotential height and winds reveal

Table 1 Most destructive hurricanes affecting Puerto Rico and Hispanola since 1960

Date	Year	Name
27 Sept	1963	Edith
29 Sept	1966	Inez
10 Sept	1967	Beulah
31 Aug	1979	David
11 Sept	1988	Gilbert
10 Sept	1996	Hortense
22 Sept	1998	Georges

Table 2 Hurricanes changing intensity near Puerto Rico since 1976

Intensify	Decay
5 Aug 1980	1 Sep 1979
24 Sep 1985	18 Sep 1989
12 Aug 1995	27 Aug 1996
12 Sep 1999	21 Sep 1998
9 Sep 2004	13 Sep 2003

interactions between sub-tropical troughs/ridges and Caribbean hurricanes via wind shear and steering flow. Its adjustment to latent heating in hurricane convection can be a useful indicator of structure but is likely to be underrepresented in NCEP reanalysis data. For purposes of describing the large-scale kinematic forcing, we analyze the upper divergent and lower rotational circulation (velocity potential and stream function, respectively).

To study the role of Saharan dust plumes in Caribbean hurricane intensification, we extract satellite estimated aerosol optical depth (AOD) from the total ozone mapping spectrometer (TOMS) and make composites for intensify and decay groups similar to Jury and Santiago (2010). A study of wind shear influence on Caribbean hurricane intensity was carried out using NCEP daily zonal wind time series averaged over the southern Caribbean (10–15N, 60–80W). We compute the wind shear by subtracting 850–700 layer from 200 hPa level and impose a Hilbert-wavelet-filter that extracts 20–60- and 300–420-day bands corresponding to the Madden Julian Oscillation (MJO) and annual cycle, considered to be most influential. We compare these environmental time series with an index of normalized hurricane intensity (Vmax/Vmean) + (Pmean/Pmin), similar to that described earlier. Two hurricane events are selected for case study analysis, and time-longitude hovmollers are averaged over 12–15N latitude to identify key features. We analyze satellite-derived rainfall from the Global Precipitation Climatology Project (GPCP) and Tropical Rainfall Monitoring Mission (TRMM) and microwave SST, together with NCEP reanalysis zonal wind, specific humidity, and absolute vorticity.

In the period 2000–2010, we analyze the performance of numerical model track forecasts using data from the NHC Automated Tropical Cyclone Forecast (ATCF) database. The ATCF was developed by the Naval Research Laboratory and provides numerical model forecasts and hurricane observations (Sampson and Schrader 2000). For this part of our study, the ATCF-HURDAT best track and intensity data were obtained and compared with model track forecasts at 48-h lead time. Seven models were available: the statistical-dynamical model (SHIP), four global dynamical models (EMX, GFS, NGPS, UKM), and two regional dynamical models (GFDL and HWRF). Brief comments are provided for each model. GFS (and AVN) is the US National Weather Service Global Forecast System, and its earlier version the Aviation model and is initialized using 3-D variational gridpoint statistical interpolation (GSI). It has a resolution of 35 km (80 km in AVN) and is a hydrostatic spectral model. EMX is the European Center for Medium-range Weather Forecasting model that is also global dynamical and hydrostatic spectral type, but is initialized with 4-D variational data assimilation. It has a horizontal grid spacing of 25 km and is the most computationally 'expensive' of the suite of operational models used by NHC in 2010. GFDL is the Geophysical Fluid Dynamics Hurricane Model designed exclusively for tropical cyclone (TC) prediction. This regional TC dynamical model is triply nested grid-point model with spatial resolutions of 30, 10, and 5 km. It is coupled with a high-resolution version of the Princeton Ocean Model (POM), which is three-dimensional with 23 vertical levels in the Atlantic Ocean. HWRF is the Hurricane Weather Research and Forecasting model, another regional TC dynamical and ocean-coupled model available since 2007. Similar to GFDL, it is run for up to four TCs every 6 h and uses a nested grid system, with spatial resolutions of 27 and 9 km for the outer and inner nest, respectively. It is coupled with the high-resolution POM and is initialized using GSI 3-D Var data assimilation. NGPS is the Navy Operational Global Atmospheric Prediction System, which is a global dynamical and hydrostatic spectral model. Its horizontal grid spacing is ~55 km. This model inserts an artificial TC vortex into its initial fields, which is created by adding synthetic data points to the observational data that are then incorporated during the 3-D Var and NRL Atmospheric Variational Data Assimilation process. SHIP is the Statistical Hurricane Intensity Prediction scheme based on statistical relationships between storm behavior and environmental conditions (e.g., SST) estimated from dynamical models, climatology and persistence. It has proven to be useful for hurricane intensity guidance. UKM is the United Kingdom Meteorological Office model, the final global dynamical. It is the only global model considered here that has non-hydrostatic physics, but as NGPS, it inserts a synthetic TC vortex. It uses a 4-D Var data assimilation scheme. We compare observed and 48-h forecast positions for 10 hurricanes in the years 2000–2010 that moved near Puerto Rico (Tables 5 and 6). The comparison is made in four time periods, D−2, D−1, D−0, and D+1, where D−0 refers to the day when the hurricanes were closest to Puerto Rico.

Our results are divided into five sections: (1) background and event impacts, (2) synoptic conditions of composite hurricanes, (3) synoptic controls on changes in hurricane intensity, (4) case studies focusing on key features, and (5) comparison of observed and model track forecasts near Puerto Rico.

3 Results

3.1 Background and impacts

While Caribbean rainfall in early (May) and late summer (October) is driven by westerly troughs (Jury et al. 2007); it is the August–September hurricane events that bring destruction. In the period 1951–2005, an average of 1.2

hurricanes/year passed through the region (σ=1.4). The average number of days/year with a hurricane in the Caribbean was 7.0 (σ=6.6). About once every 4 years, hurricanes are rare. Kimball and Mulekar (2004) have demonstrated that more intense hurricanes tend to track westward across the Antilles, while weaker tropical storms recurve poleward across the western Atlantic. There are two dominant tracks for hurricanes near Puerto Rico (www.nhc.noaa.gov). The first occurs with ~20% frequency and is oriented westward along 15N. It tends to be composed of hurricanes originating near Africa, passing south of Puerto Rico headed toward the Gulf of Mexico. The second is more frequent (~30%) and oriented northwestward, with hurricanes forming north of Puerto Rico (22N) and affecting the Atlantic seaboard of the USA. Hurricane tracks directly over the Greater Antilles Islands are less frequent (<10%) and are the subject of this study (Fig. 1). The HURDAT pressure and wind records indicate that David, Inez and Beulah were most intense. Synoptic weather reports and damage estimates for the seven identified hurricane cases are given below, based on NHC/TPC bulletins and national summary reports.

Hurricanes Edith (1963), Inez (1966), and Beulah (1967) occurred prior to the modern era of satellite coverage and will not be discussed in much detail. Edith crossed St Lucia on 25 September 1963 with highest winds of 44 m/s. In Puerto Rico, the most damage was along the south-facing coast, with residential damage >US$2 M and agricultural losses of US$3 M (adjusted to year 2000), with swells of 5 m and surges of 3 m, winds of 33 m/s and rainfall up to 230 mm. Hurricane Inez in 1966 propagated westward across the tropical Atlantic, followed by rapid intensification as the system skirted a strong North Atlantic anticyclone. The hurricane Pmin was 927 hPa with winds >55 m/s recorded on 27 September just before landfall over the Dominican Republic. Damage reports (Table 3) indicate great losses with over 1,000 deaths, although the hurricane was considered "small" (Hawkins and Imbembo 1976). Hurricane Beulah in 1967 reached a central pressure of 947 hPa just southwest of Puerto Rico (17N, 69W) on 10 September with sustained winds of 66 m/s. At that time, movement was 290° at 2.6 m/s. Later, the storm veered westward, remaining in the Caribbean. NHC reports emphasize negative impacts downstream over the Yucatan and Gulf of Mexico.

Hurricane David in 1979 was considered a "Cape Verde" hurricane, starting as an African easterly wave and propagating around the perimeter of a sub-tropical ridge. The hurricane passed over Dominica with winds of 64 m/s, 250 mm of rain, >50 deaths, and 60,000 people (75% of population) made homeless. Crop damage was said to be US$50 M on Martinique and US$100 M on Guadeloupe, where 5 m swells were reported. Hurricane David flooded Puerto Rico with rainfall up to 500 mm on 31 August. It recurved briefly near Hispanola as an upper trough moved eastward near Florida. A pressure of 924 hPa and winds of 77 m/s were reported by aircraft near the eye (Hebert 1980). David caused over 1,000 deaths and agricultural losses ~US$2.8 B in the Dominican Republic. Further damage reports were noted in the Bahamas where >200 mm of rainfall was measured.

Hurricane Gilbert in 1988 tracked westward across the Caribbean reaching a pressure of 900 hPa near Jamaica on 14 September with coastal winds of 64 m/s, a 3-m surge and 9-m swells observed. Black and Willoughby (1992) provide an account of this hurricane. Deaths were 45

Fig. 1 Tracks of seven major hurricanes affecting Puerto Rico and Hispanola since 1960 from HURDAT, with colors for strength: above cat 2 (*red*), cat 1 (*yellow*), below cat 1 (*green*). *Dot* is D−0 point

Table 3 Damage estimates: Hurricane Inez 1966

Location	Deaths	(US$ Millions)[a]
Guadeloupe	27	265
Dominican Rep	~100	65
Haiti	~750	55
Bahamas	5	80
Cuba	50	100
Eastern Mexico	65	530
Storm Total	~1000	1120

[a] Adjusted to year 2000 US$

(losses ~US$3.6 B) in Jamaica, 30 in Haiti, five in Dominican Rep, three in Puerto Rico, and five in Venezuela. Mexico suffered significant damage as Gilbert continued westward.

Hurricane Hortense in 1996 developed near the Cape Verde Islands on 31 August and continued westward around the periphery of a strong ridge. It passed over Guadeloupe with significant rains, but surface winds were below hurricane strength under westerly shear. After slowing down, Hortense took a turn northwest and moved over Puerto Rico (Pasch and Avila 1999). Rainfall up to 600 mm was reported on 10 September with landslides resulting in 21 deaths, 12,000 homes destroyed, and >US$150 M in damage. Similar damage estimates were reported in the Dominican Republic, where a 3-m storm surge was observed and 80% of crops were leveled. The hurricane continued northwesterly across the Bahamas producing 57 m/s winds and a pressure of 935 hPa on 13 September.

Hurricane Georges in 1998 also originated from an African wave and moved on a persistent westerly track for 10 days in response to a mid-level ridge. Georges reached hurricane intensity on 17 September. By the 21st winds up to 68 m/s were reported by aircraft, while intensity varied due to wind shear (Pasch et al. 2001). It tracked across Antigua and made landfall over Puerto Rico with winds of 46 m/s and a storm surge of 3 m on the southeast coast. Hurricane Georges produced the highest rainfall observed at Puerto Rico in the twentieth century. The eye passed over Santo Domingo, where it generated 900 mm of rain resulting in landslides and many deaths (Table 4). The hurricane tracked along the north coast of Cuba producing rainfall of 600 mm. It struck Key West on 25 September with winds of 44 m/s and a storm surge of 2 m (Tables 5 and 6).

Table 4 Damage estimates: Hurricane Georges 1998

Location	Deaths	(US$ Millions)[a]
Antigua	2	?
St. Kitts and Nevis	4	~400
U.S.Virgin Islands	0	50
Puerto Rico	0	1750
Dominican Rep.	380	~1000
Haiti	209	?
Storm Total	602	> 3000

[a] Adjusted to year 2000 US$

3.2 Synoptic environment of composite hurricane

In this section, we analyze composite features for the seven hurricanes. Figure 2a reveals a band of SST >29°C across the southern Caribbean from Venezuela to the hurricane track ~17N. The additional thermodynamic energy helped draw the hurricanes south of their mean track (~22N near Puerto Rico, Elsner et al. 2000). Composite NCEP rainfall (Fig. 2b) was 30 mm/day, whereas ~100 mm/day was observed over Puerto Rico. Convective rainfall extended ~200 km from the center and was greatest in the NE sector (19N, 68W). The precipitable water pattern indicates that moisture is sourced from the south (Fig. 2c). There is a band of low precipitable water east of the Bahamas (25N) indicative of a ridge line on the poleward side of the composite hurricane that amplifies latent heat flux (>240 $W m^{-2}$, Fig. 2d).

Figure 3a illustrates the upper 200 hPa wind pattern during Caribbean hurricane passage and highlights a broad ridge in the westerly flow over the northwest Atlantic (30–40N) with a SW trough over the US east coast (Fig. 3c) where moisture is present (Fig. 2c). The composite low level 925 hPa winds around the hurricane are about ~30% of the observed values (55 m/s), related to dispersion among the seven cases (Fig. 1b). There is a cyclonic minimum near 17N, 70W surrounded by a ring of strong easterly winds on the northern flank. The composite

Table 5 HURDAT intensity data at D−1, D0 and D+1

Storm ID	D−1		D0		D+1	
	Vmax	Pmin	Vmax	Pmin	Vmax	Pmin
Fabian03	60 m/s	945 hPa	55	945	52	944
Frances04	55	946	60	941	60	939
Ivan04	57	950	65	938	65	923
Jeanne04	25	996	30	991	32	988
Emily05	37	991	57	952	60	953
Dean07	45	967	72	923	62	923
Felix07	17	1007	32	992	65	935
Ike08	52	954	47	965	55	947
Omar08	32	983	47	970	32	986
Earl10	42	971	57	938	55	940

Table 6 HURDAT position data at D−1, D0, and D+1

Storm ID	Lat D−1	Lon D−1	Lat D0	Lon D0	Lat D+1	Lon D+1
Fabian03	19.6	−59.2	21.3	−61.8	23.8	−63.3
Frances04	19.6	−60.7	20.6	−66.4	22.2	−71.4
Ivan04	12	−62.6	13.3	−68.3	15.2	−72.8
Jeanne04	16.7	−63.5	18.1	−66.2	18.8	−69
Emily05	11.9	−61.5	13.7	−68.4	15.4	−75
Dean07	14.4	−61.7	15.4	−68	16.8	−74.3
Felix07	12.1	−59.4	12.6	−66.1	13.8	−73
Ike08	23.5	−61.9	21.9	−67.7	21	−72.8
Omar08	14.1	−68.3	16.7	−65.2	22.8	−58.8
Earl10	17.7	−60.6	19.6	−65.3	22.5	−69.4

hurricane is large and consistent with the annular cases described by Knaff et al. (2003). The accompanying velocity potential and streamfunction fields in Fig. 3b and d reveal interactions between the hurricane and the large-scale circulation. The divergent circulation (Fig. 3b) maintains the westward track so hurricanes pass over the Antilles Islands leaving a path of destruction. The anticyclonic streamfunction associated with the North Atlantic high guides African easterly waves into the Caribbean. West of 75° W the 925 hPa streamfunction becomes cyclonic, opening a path toward Cuba.

Figure 4 illustrates a N–S slice through the hurricane for composite zonal and meridional wind, vertical motion, and vorticity. Easterly flow on the northern flank of the

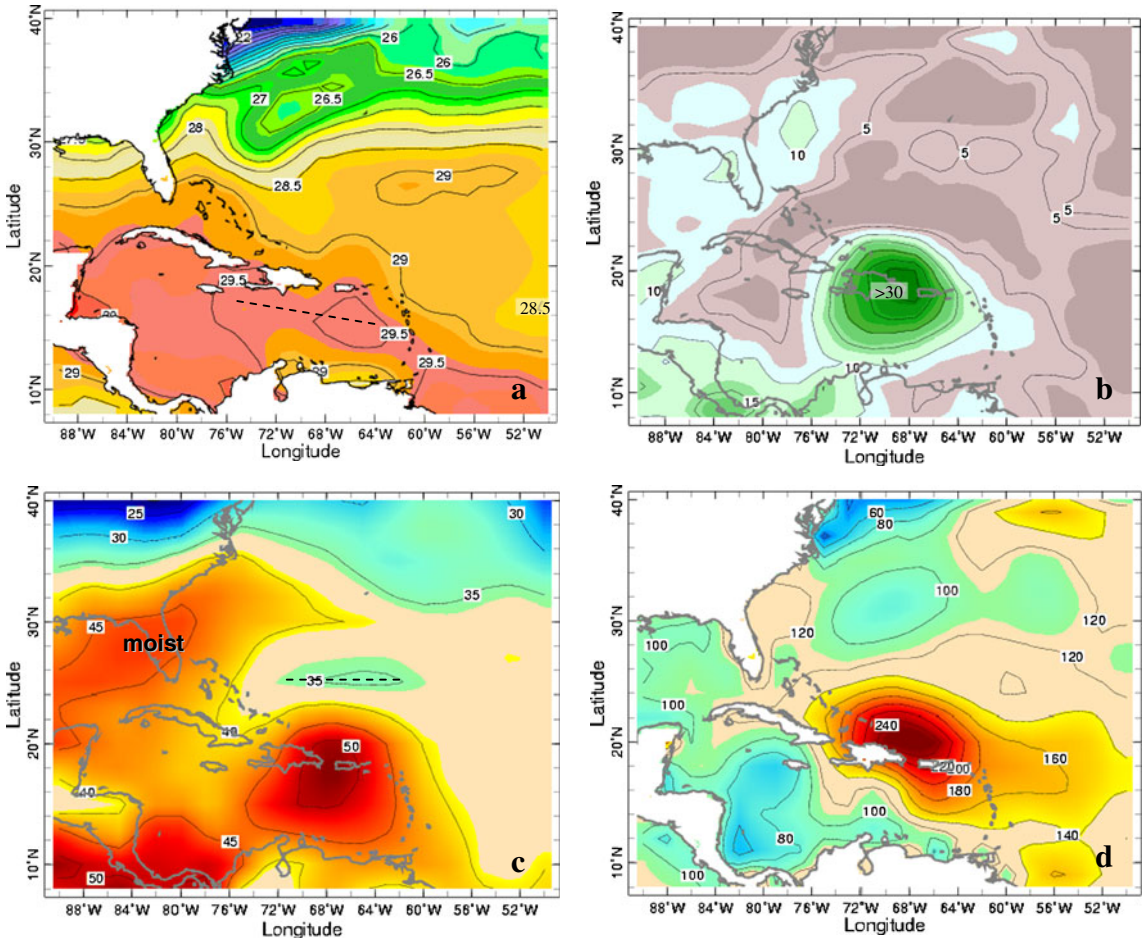

Fig. 2 Composite daily **a** oi-SST, **b** NCEP convective rain rate (mm/day), **c** NCEP precipitable water, and **d** NCEP latent heat flux. *Dashed lines* highlight important features

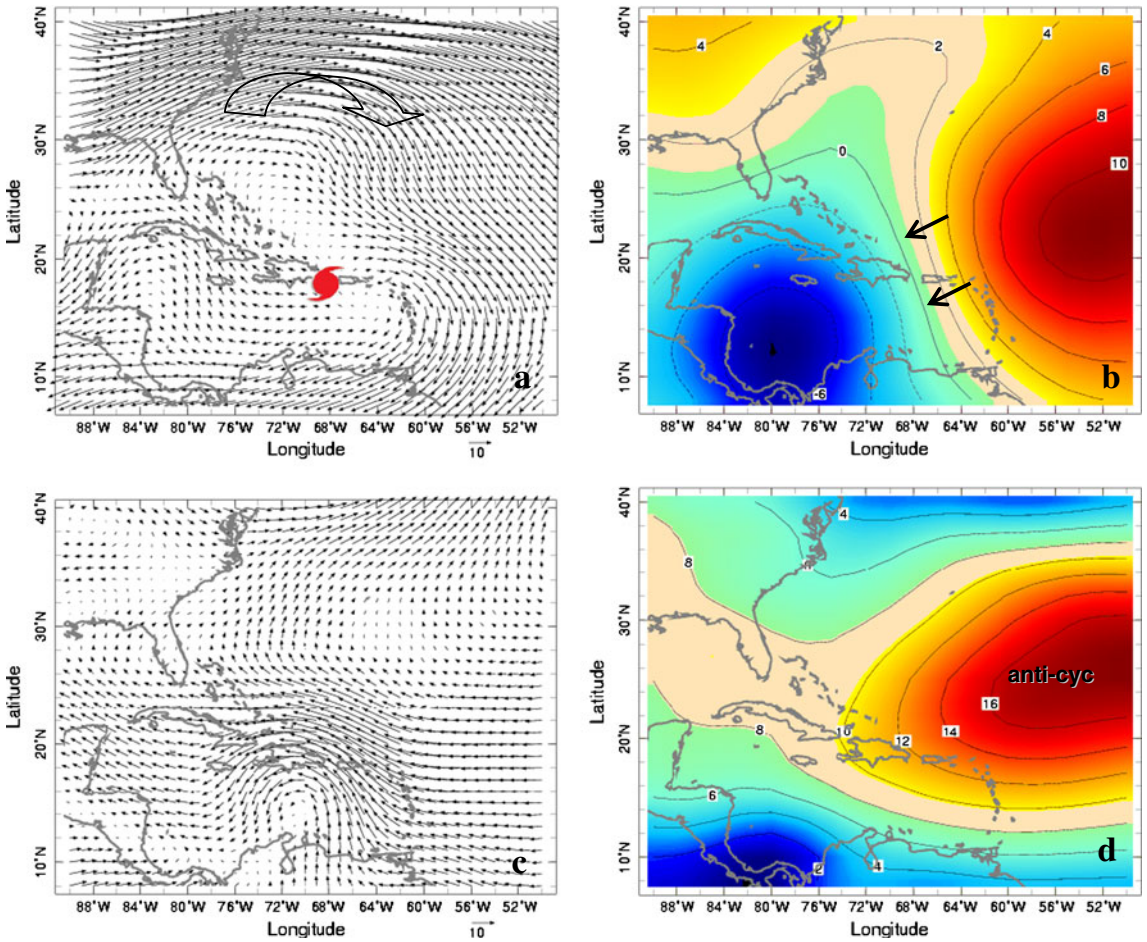

Fig. 3 Composite daily NCEP **a** 200 hPa wind vectors, **b** 200 hPa velocity potential ($m^2/s \times 10^6$), **c** 925 hPa wind vectors and **d** 925 hPa streamfunction ($m^2/s \times 10^6$). Vector key is given

composite hurricane is well captured but westerlies on the southern flank are weak. Above 300 hPa, north of 25N the westerly sub-tropical jet is evident. Vertical uplift is slanted poleward, reaching a maximum around 500 hPa (Fig. 4b). Southerly winds are noteworthy below 500 hPa and absolute vorticity $>8 \cdot 10^{-5}$ s^{-1} prevails across the system 16–19N. In the following section, we analyze how the environment affects hurricane intensity near Puerto Rico.

3.3 Hurricane intensity

Table 2 lists the case dates pertaining to this analysis, while Fig. 5a and b plots their 6-h displacements from Day−1 to Day+1. The intensifying (decaying) cases propagate at 290° (300°). Decaying cases tend to pass over the Antilles Islands while intensifying cases track around them, pointing to frictional influences. The change index is plotted against longitude in Fig. 5c. The two sets of cases show differences east of Puerto Rico (65° W), but west of 72° W (Hispanola) there is little to separate them. The composite difference field for 200 hPa geopotential height (Fig. 6a) indicates that intensification depends on an upper ridge over the Gulf Stream (Bermuda) which promotes a westward hurricane track over warmer water. It is found that decaying cases gradually loose the Pmin "bulls-eye" shape and elongate toward Florida (not shown). The 925 hPa wind difference field shows an anticyclonic gyre behind the system (Fig. 6b), while SSTs are ~0.5°C warmer in the Caribbean in agreement with Emanuel (2005). The satellite OLR difference field (Fig. 6c) has positive values east of the Bahamas (25N) coincident with low rainfall and precipitable water (cf. Fig. 2b and c). Thus for hurricane intensification, convective bands on the poleward flank are a key determinant as suggested by McBride and Zehr (1981).

These aspects are further studied as vertical sections in Fig. 7. In the east–west dimension, a low-level positive geopotential height anomaly is located ~1,000 km behind the system. In that area, there is sinking motion and negative specific humidity differences. Negative height differences in the composite hurricane link with an upper level trough to the west, where enhanced easterly outflow is found. In the north–south section, the pattern is dominated

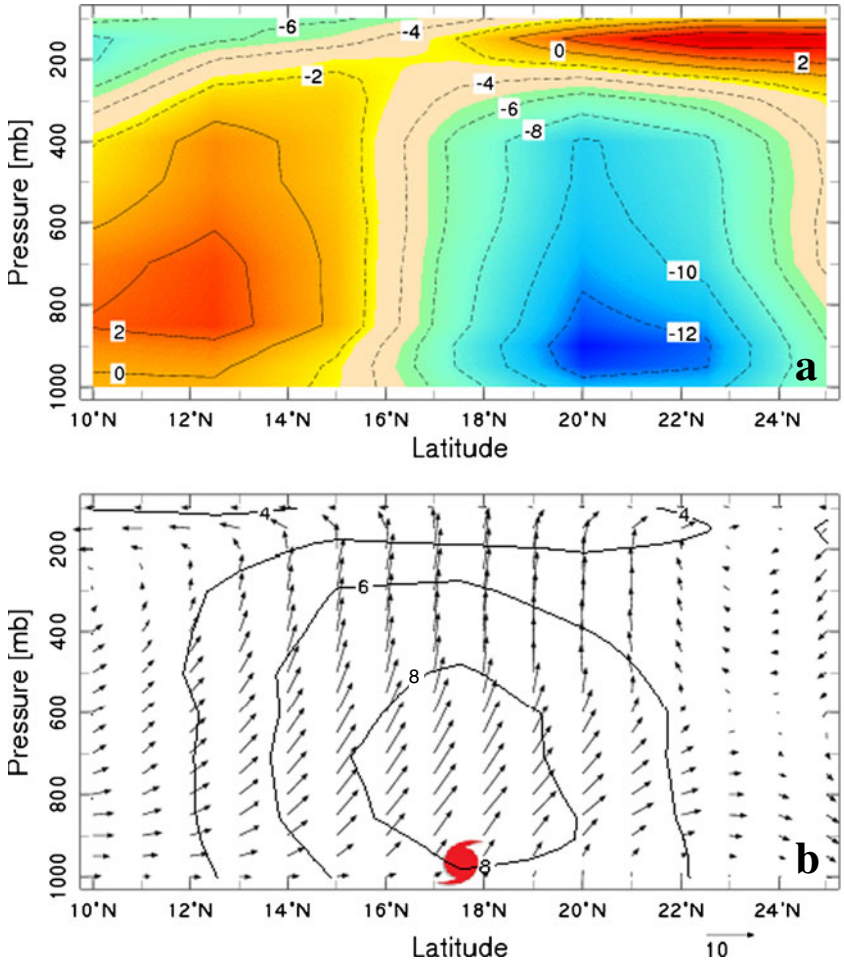

Fig. 4 N–S slice through the composite hurricane for **a** zonal wind (m/s) and **b** meridional wind, vertical motion × 10 (vectors m/s) and absolute vorticity × $10^{-5}s^{-1}$ (contour)

by a meridional overturning cell that is more coherent on the poleward flank which links with an upper ridge in the mid-latitudes. It is pointed out that this set of composites has limited representativity.

Recent studies indicate that Saharan dust can suppress Atlantic hurricanes through mid-tropospheric heating, subsidence and less efficient cloud condensation (Jury and Santiago 2010). So we make an analysis of AOD anomalies from the TOMS satellite. In Fig. 8, the composite AOD field for intensify cases has values in the range 0.6 in the hurricane path, while the decay cases are surrounded by AOD anomalies ~0.9. The Saharan dust plume extends more into the Caribbean in the decay composite. Yet, both composites demonstrate that considerable dust accompanies Caribbean hurricanes from West Africa.

3.4 Hurricane case studies

We study the coherence of moisture advection in the southern Caribbean, using hovmoller plots (Fig. 9) of zonal wind and specific humidity over the period 5 days before and after intensity change for two cases: 5 Aug 1980 (Allen) and 27 Aug 1996 (Edouard). In the intensifying case the moist westerlies equatorward of the hurricane are well organized, whereas in the decaying case the westerlies are spread out and considerably drier. Both exhibit westward propagation consistent with the hurricane to the north, but easterlies behind the system are found only in the intensifying case.

We investigate how kinematic oscillations affected hurricanes in the 1979 and 1998 summers, using NCEP hilbert-wavelet-filtered daily zonal wind shear (200–700/850 hPa) averaged over the southern Caribbean (10–15° S, 60–80° W). ~40- and ~365-day cycles are compared with an index of normalized hurricane intensity. Figure 10a and b provides a yearlong analysis of wind shear with embedded hurricane events. In David 1979, the annual cycle has a typical inverted Gaussian shape centered on the hurricane season. Easterly (negative) shear neatly contains an envelope of ±45-day oscillations that amplify during the hurricane season. In Georges 1998, the annual cycle was asymmetric-recovering from a strong El Niño that produced a strange biannual oscillation of zonal wind shear. Similarly the MJO cycles started the summer weak and fast (±30 days), later growing in amplitude and phase. The

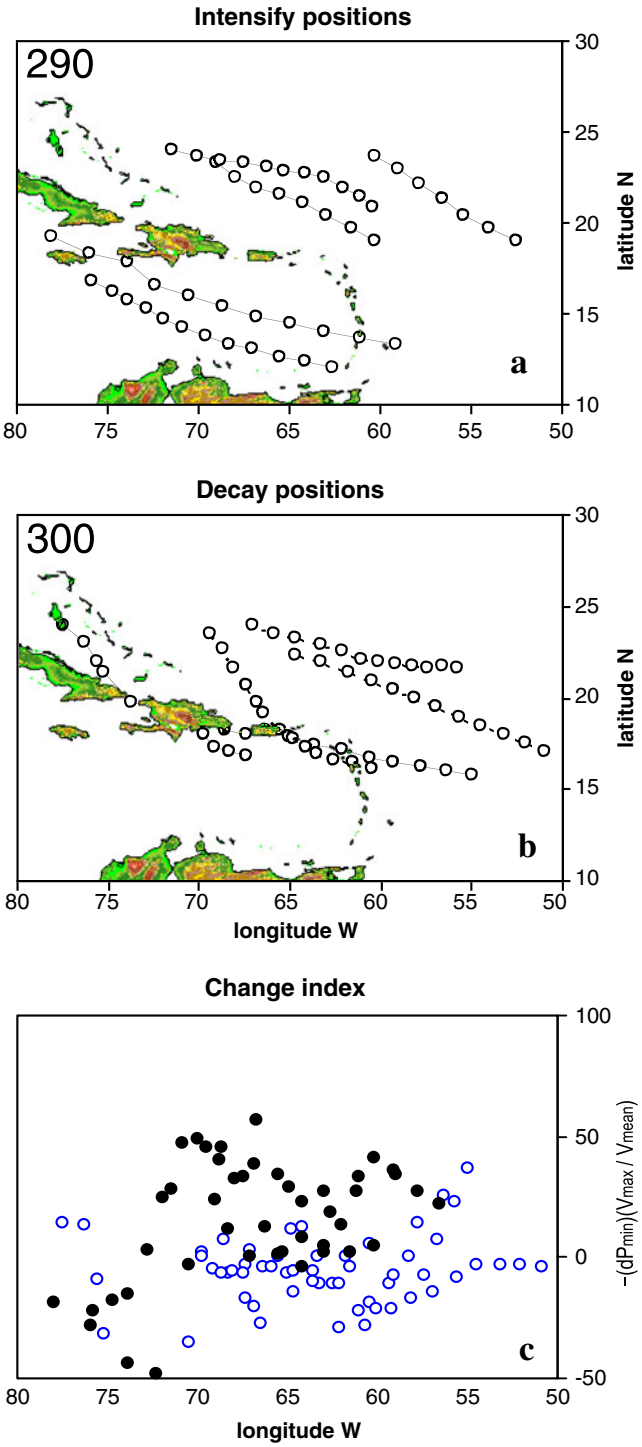

Fig. 5 Map of hurricane center points at 6-hr intervals from Day−1 to Day+1 for intensifying (**a**) and decaying (**b**) cases; *number highlights* mean direction. **c** Change index values vs. longitude for intensify (*solid*) and decay cases

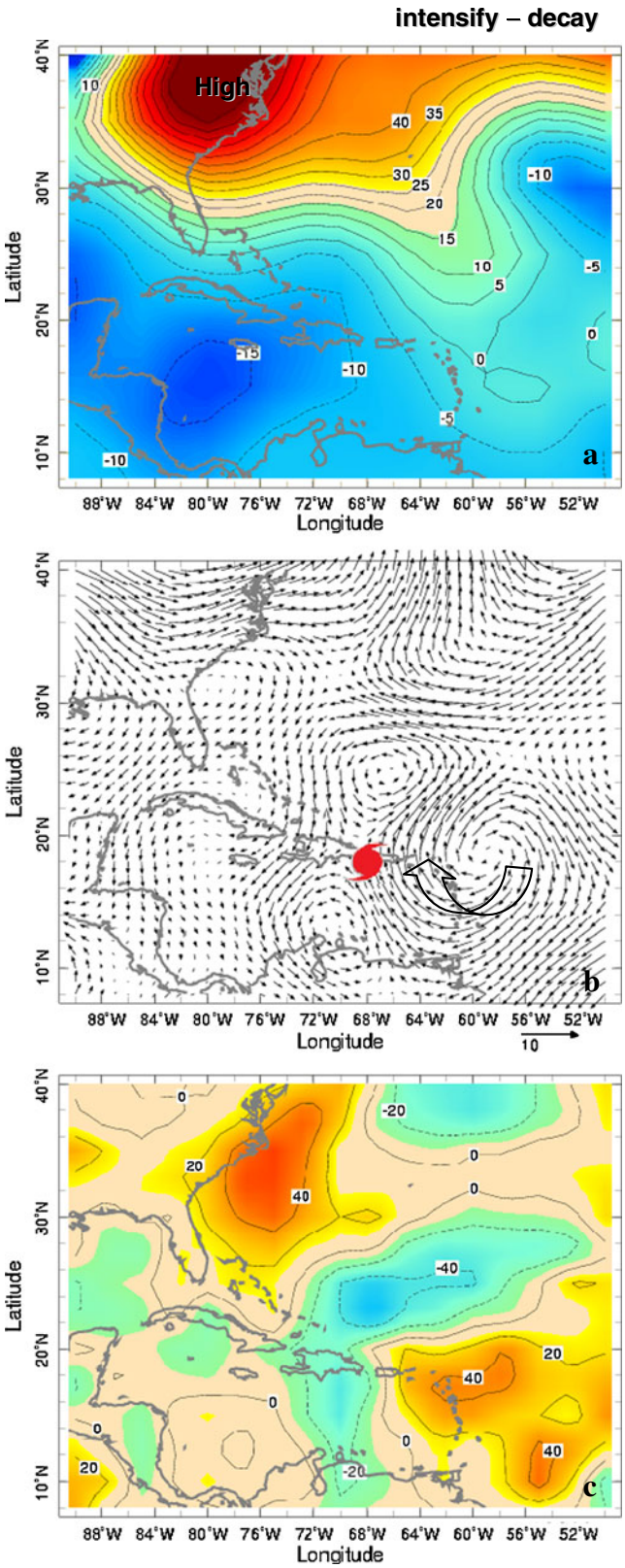

Fig. 6 Composite NCEP intensify minus decay difference fields: **a** 200 hPa geopotential height (m), **b** 925 hPa wind vectors (with vector key) and composite hurricane position, **c** NOAA satellite OLR (W/m^2)

hurricanes intensify when both MJO and annual cycles come into easterly shear. Ferreira et al. (1996) describe how MJO surges generate cyclonic vorticies in the ITCZ, while Wong and Chan (2004) relate how it affects hurricane

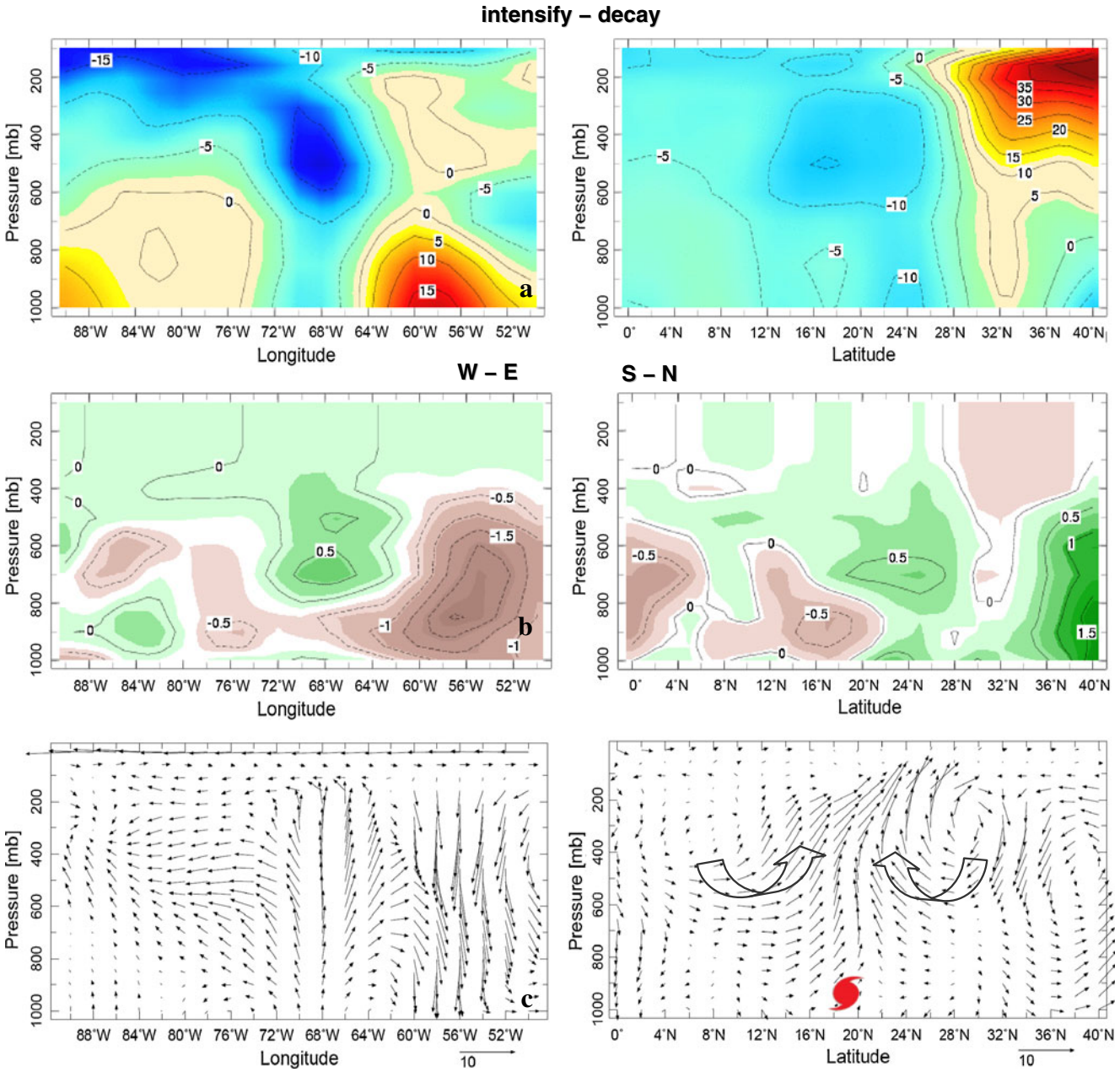

Fig. 7 Composite NCEP intensify minus decay difference fields, *left* E–W slice, *right* N–S slice through the hurricane: **a** geopotential height (m), **b** specific humidity (g/kg), and **c** U,V wind/vertical motion × 100 (vectors m/s)

intensity. Here evidence implicates the MJO as one of the drivers of Caribbean hurricanes, in agreement with Maloney and Hartman (2000).

The most destructive hurricane to affect Puerto Rico in the past century was hurricane Georges. Key features of its environment are identified in Fig. 11. Like most Caribbean hurricanes, it originated from an African easterly wave. Hovmoller analysis of rainfall and vorticity along 15N (Fig. 11a) reveals the system formed over the Ethiopian highlands coincident with a Nile flood event at the end of August 1998 that caused the level of Lake Tana (area 2,150 km^2) to rise >1 m. The wave tracked westward from Africa changing strength and speed, and hit Puerto Rico on 21–22 September. At that time, there was inflow from the southeast (Trinidad) over SST >30°C and vegetation >0.8 (Fig. 11b, c). Upwelling along the coast of Venezuela was weak (~29°C) due to a spell of reduced trade winds. In the lee of the Antilles island chain, SST were >31°C. TRMM rainfall of 100 mm/day was observed along the hurricane track, reaching 200 mm/day southeast of Puerto Rico. GFS 24 h rainfall forecasts in the same period were four times lower and tended to spread cross-latitude to the west.

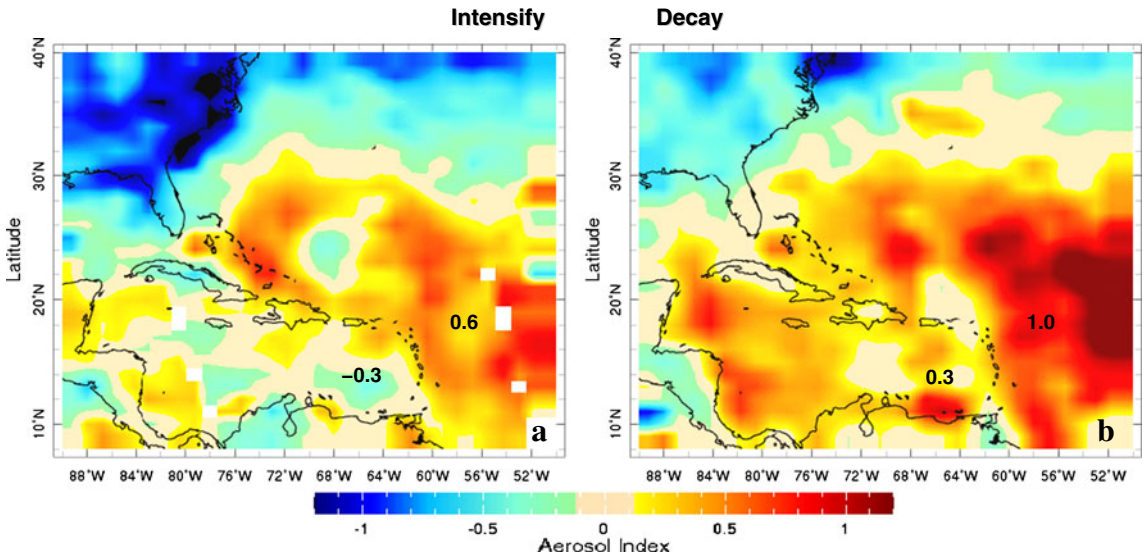

Fig. 8 Composite TOMS aerosol optical depth anomalies for: **a** intensify and **b** decay cases, shaded with values at key points labeled

3.5 Hurricane track forecasts 2000–2010

Analysis of numerical model 48-h forecasts and observed hurricane positions are given in Fig. 12. There is a trend in the forecast errors from an east to north bias as these pass Puerto Rico. At D−2, the ensemble mean position error (MPE) is +1.0° longitude to east; hence, the models forecast slower westward movement of the hurricane than was observed. By D−1 the MPE changes to +1.1° latitude to north, indicating the models favor an Atlantic track over the observed Caribbean. At D0 when the hurricanes are closest to Puerto Rico, the model track forecast skill is

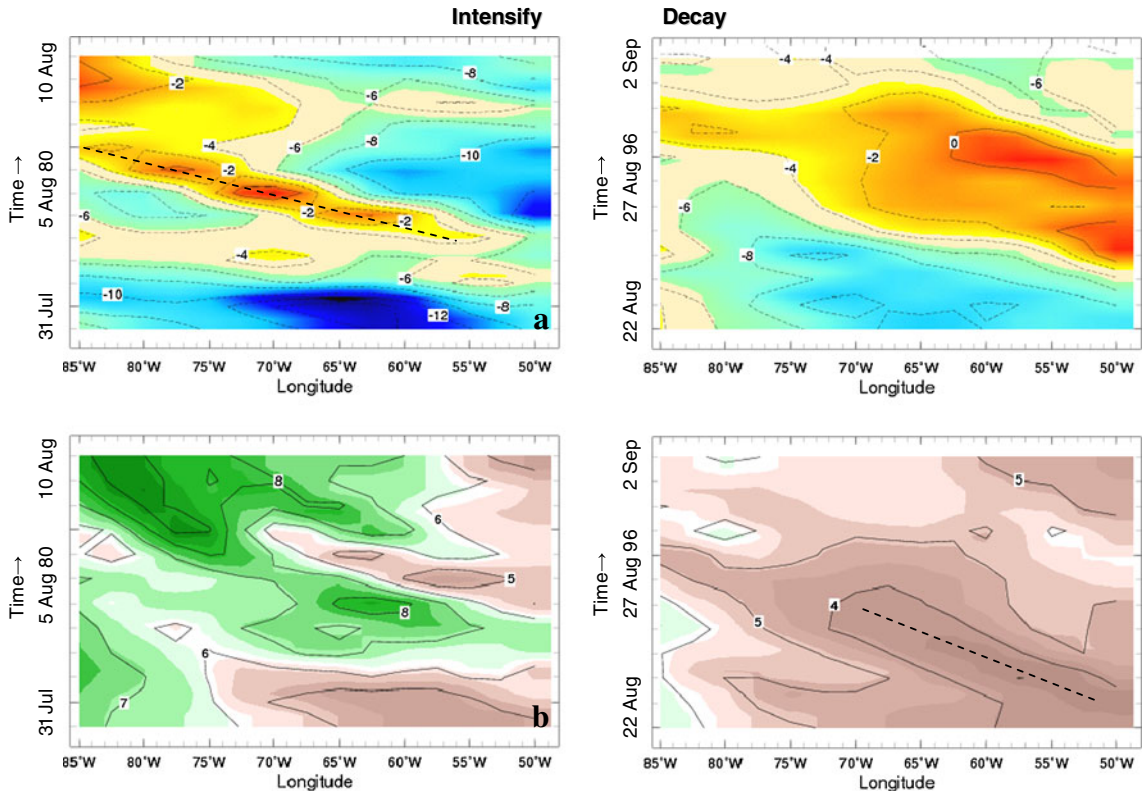

Fig. 9 Case study time-longitude hovmoller averagd over 12–15N of **a** 700 hPa zonal wind and **b** 700 hPa specific humidity for intensify case (*left*) and decay case (*right*). *Dashed lines* highlight westward propagation

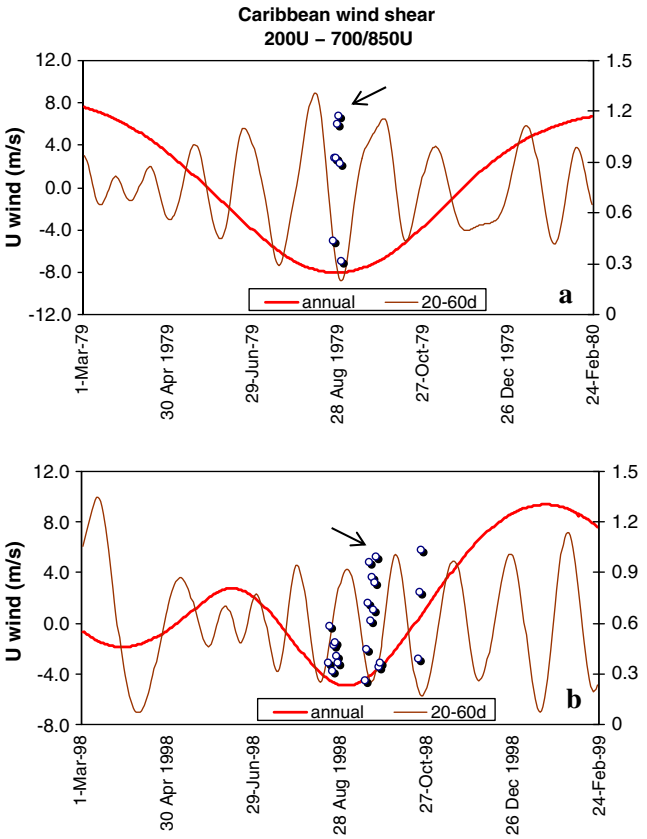

Fig. 10 Caribbean wind shear at annual (*red line*) and MJO time scales, versus normalized hurricane intensity (*dots*) for **a** David 1979, and **b** Georges 1998 (*arrows*). Positive refers to westerly shear; intensity of 1 = cat.5

better, with a MPE of +0.69° latitude, −0.095° longitude, a slight north bias. Finally, at D+1 the ensemble position error is +0.68° latitude, −0.34° longitude, a northwest bias. A full evaluation of factors underlying the forecast discrepancies near Puerto Rico is beyond the scope of this paper, but we speculate that model representation of steering flow in the eastern Caribbean and hurricane interaction with Antilles islands are likely candidates. Composite analysis for the hurricanes studied in this section indicate a zone of 500 mb easterly flow >10 m/s that extends to Africa (not shown). If the models under-represent these easterlies, then hurricanes are forecast to move slower than observed at D−2. As the hurricanes approach Puerto Rico at D−0, the models improve on that point, possibly related to Antilles radiosonde and AMDAR profile data, and Meteo-France Antilles radar data. By D+1, the models forecast the hurricanes to be more northwest than observed, suggesting the frictional drag over the Antilles is underrepresented. Another large-scale influence could be the North Atlantic anticyclone and the Bernoulli effect of South America that accelerates easterlies in the Caribbean. A composite analysis of SST for this group of ten cases confirms a +0.8°C anomaly east of the Caribbean.

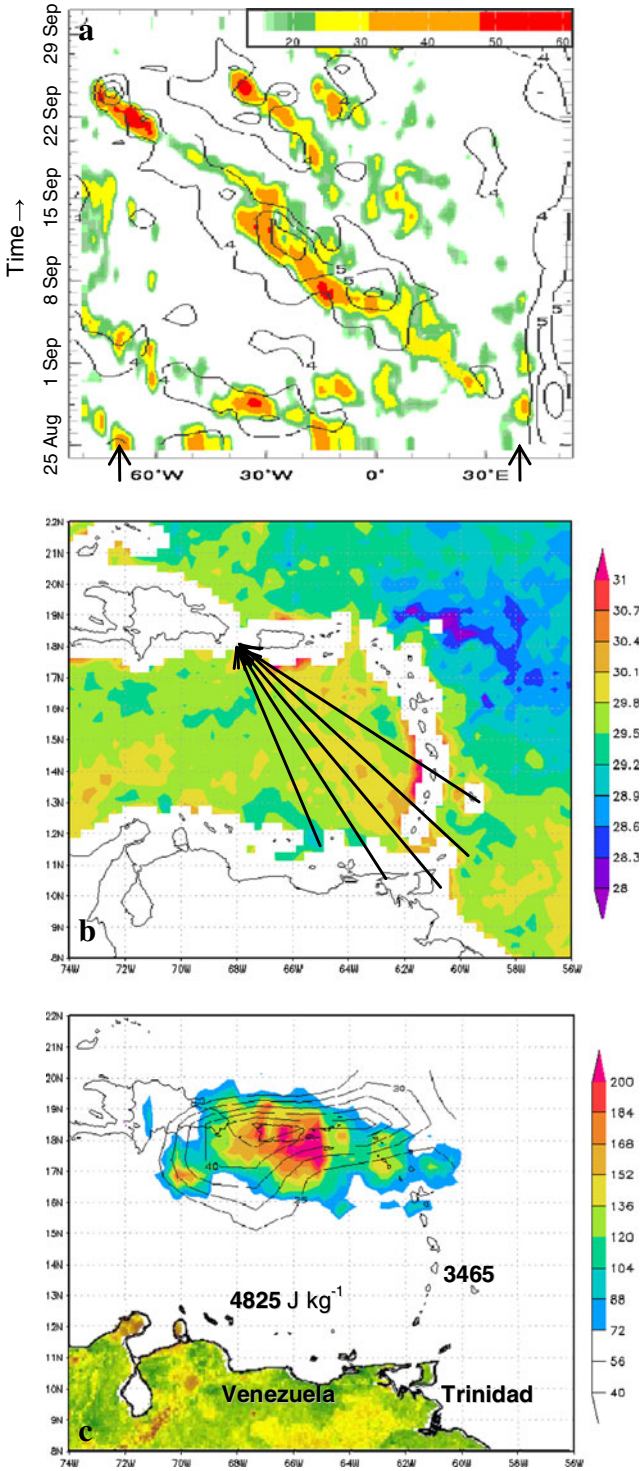

Fig. 11 Georges case study: **a** Hovmoller time longitude plot along 15N of GPCP rainfall (*shaded* mm/day) and NCEP 700 hPa absolute vorticity (contour×$10^{-5}s^{-1}$) with *arrows* for Puerto Rico and Ethiopia. 21–22 September 1998 maps of **b** TMI SST and dominant air trajectories at 925 hPa and **c** TRMM rainfall (*shaded*) and GFS 24 h forecast rainfall (contour, mm/day) with low values omitted. Radiosonde CAPE values are given, South American vegetation *shaded* 0.1–0.9

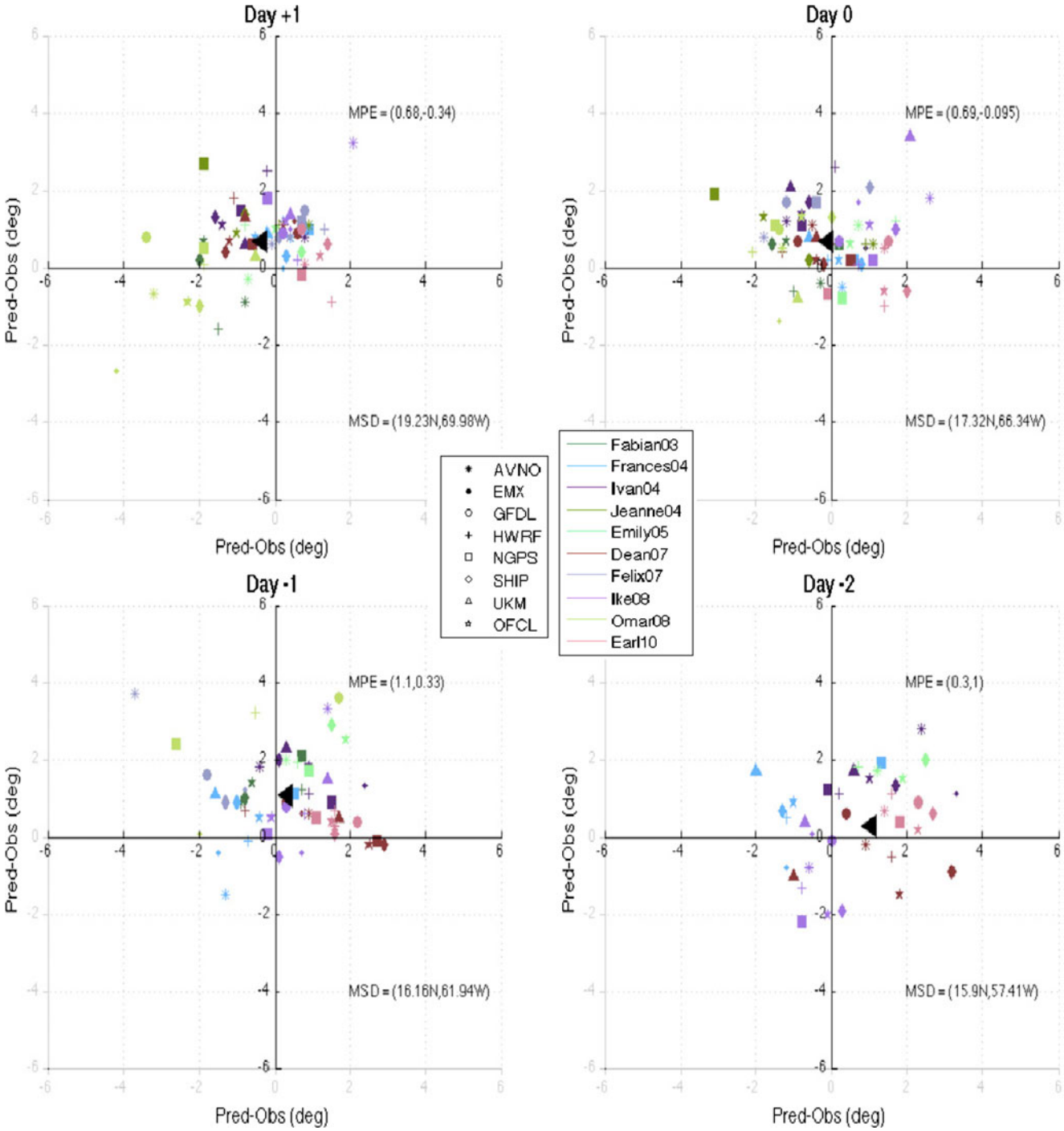

Fig. 12 Scatterplots of position (lat/lon) for hurricanes that moved close to PR in the period 2000–2010. *Colors* represent a storm; *symbols* represent a model—as per keys. The NHC official forecast is the *small star* per case. The *large black triangle* represents the ensemble forecast position. The observed position is the center of the scatterplot with mean coordinates: MSD. MPE is given. D−2, D−1, D−0, and D+1 refer to intervals when the storm is two and 1 day before arrival at Puerto Rico, and on arrival and 1 day after

4 Discussion and summary

Tropical easterly shear favors hurricane development via asymmetric vertical motions that enhance convection and vorticity in the equatorial flank (Fig. 4b), steering the system to the west (Tuleya and Kurihara 1981; Chan and Williams 1987; Fiorino and Elsberry 1989; Pfeffer and Challa 1992; Jones 1995; Bender 1997; Frank and Ritchie 2001; Halverson et al. 2006). Evidence for large-scale easterly shear is presented in Fig. 13a and b. The

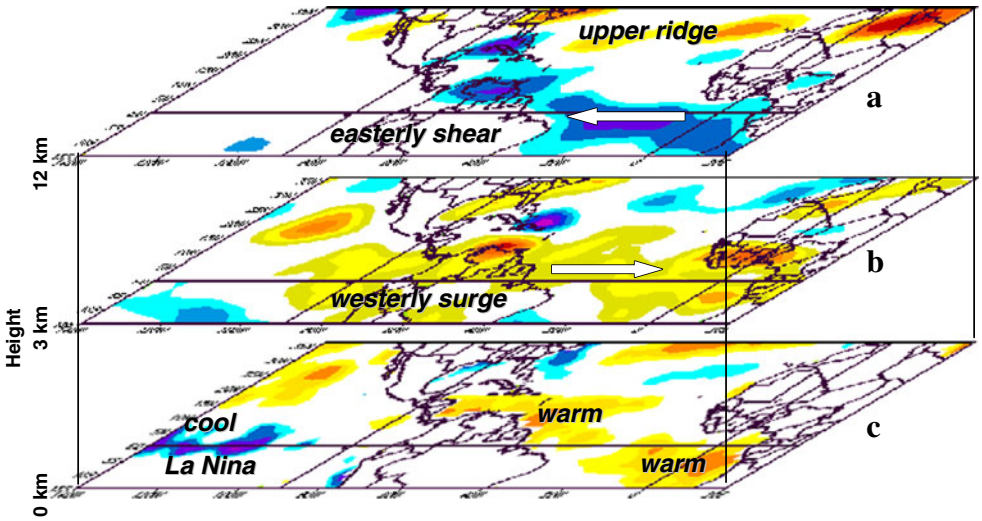

Fig. 13 Composite daily maps summarizing large-scale influences on Caribbean hurricanes, **a** 200 hPa U wind anomaly >3 m/s (*yellow*) less than −3 m/s (*blue*), **b** 700 hPa U wind anomaly >2 m/s (*yellow*) less than −2 m/s (*blue*), **c** SST anomaly >0.3°C (*yellow*) less than −0.3°C (*blue*)

composite pattern favoring Caribbean hurricanes has upper easterly flow connecting the Caribbean with the central Atlantic, and low-level westerly anomalies spread across the tropics as part of a zonal overturning MJO circulation. Although MJO are rather weak in the western hemisphere due to equatorial upwelling, Andes Mountains, and baroclinic atmosphere, a signal still persists (Fig. 10).

Analyzing sea temperatures over the wider domain (Fig. 13c), we find below normal SST in the central Pacific (La Niña) and above normal SST in the equatorial and South Atlantic Ocean. Studies have demonstrated how cool waters in the east Pacific induce upper easterly flow over the tropical Atlantic (Jury and Enfield 2010). Briegel and Frank (1997) provide a similar analysis for Pacific typhoons. Since 1950, La Niña events coincided with 12 hurricanes near Puerto Rico, whereas in El Niño events, only three were reported. Although the Pacific modulates wind shear, thermodynamic energy is dependent on local SSTs. Here, we see the equatorial and South Atlantic warming during the passage of hurricanes over Puerto Rico. An upper ridge over the Gulf Stream combines with warmer Caribbean SST to draw hurricanes across the Antilles Islands and their urban centers: San Juan, Santo Domingo, Kingston, and Havana.

Although hurricanes generate mesoscale circulations, their thermodynamic and kinematic energy is controlled by the surrounding large-scale environment. Our analysis has presented low-resolution historical evidence of composite hurricanes near Puerto Rico (18N, 68W). Seven cases were identified since 1960 when hurricanes above category two caused destruction on the islands of Puerto Rico and Hispaniola. The return interval is about 8 years. Most cases occur in early September when annual and intraseasonal oscillations of wind shear are favorable. Easterly shear usually develops over the Caribbean in late summer and is modulated >10 m/s by MJO.

Trade winds off the coast of Venezuela average ~6 m/s in the hurricane season and produce a cool upwelling plume (~27°C) that extends across the southern Caribbean. A week before passage of our composite hurricanes, trade winds decline to ~3 m/s and SST off Venezuela remain above 29°C (Fig. 2a), so destructive hurricanes are drawn equatorward. An upper ridge east of Florida ensures track-recurvature is inhibited. Sinking motions and dry air appear in an anticyclonic anomaly behind intensifying hurricanes (Figs. 6b and 7a, b). Dust levels were found to be lower (AOD <0.6) for intensifying systems. Hurricanes tend to form and strengthen with tropical near-surface westerly wind anomalies modulated by MJO that enhance cyclonic vorticity and moisture advection. Although NCEP reanalysis fields are smooth around hurricanes, we have identified a number of key features that offer guidance on changes of track and intensity in the Caribbean.

In Section 3.5, we analyzed trends in numerical model forecast errors for hurricanes passing Puerto Rico in the period 2000–2010. We found an ensemble bias that shifted from 1° east at D−2 (obs. 15.9N, 57.4W) to 1° north at D−1 (obs. 16.6N, 61.9W). The north bias was maintained at D−0 and D+1 indicating the models favor an Atlantic track, while the hurricanes often take a Caribbean track. Although the errors are small, they are significant in that hurricanes that remain south of the Antilles Islands have far greater impact than those that pass to the north. Further studies could include analysis of why models under-represent the easterly steering flow and island drag.

Acknowledgements We thank NSF Epscor for funding this project on Caribbean hurricanes at the Physics Dept, University of Puerto Rico Mayaguez.

References

Aberson SD (2001) The ensemble of tropical cyclone track forecasting models in the North Atlantic basin (1976–2000). Bull Amer Meteor Soc 82:1895–1904

Aiyyer AR, Thorncroft C (2006) Climatology of vertical wind shear over the tropical Atlantic. J Climate 19:2969–2983

Bender MA (1997) The effect of relative flow on the asymmetric structure of the interior of hurricanes. J Atmos Sci 54:703–724

Black ML, Willoughby HE (1992) The concentric eyewall cycle of Hurricane Gilbert. Mon Weather Rev 120:947–957

Braun SA (2002) A cloud-resolving simulation of Hurricane Bob (1991): Storm structure and eyewall buoyancy. Mon Weather Rev 130:1573–1592

Briegel LM, Frank WM (1997) Large-scale influences on tropical cyclogenesis in the Western North Pacific. Mon Weather Rev 125:1397–1413

Chan JCL, Williams RT (1987) Analytical and Numerical Studies of the Beta-Effect in Tropical Cyclone Motion. Part I: Zero Mean Flow. J Atmos Sci 44:1257–1265

DeMaria M, Lawrence MB, Kroll JT (1989) An error analysis of Atlantic tropical cyclone track guidance models. Weather Forecast 5:47–61

DeMaria M, Mainelli M, Shay LK, Knaff JA, Kaplan J (2005) Further Improvements to the Statistical Hurricane Intensity Prediction Scheme (SHIPS). Wea Forecasting 20:531–543

Elsberry RL (1995) Recent advancements in dynamical tropical cyclone track predictions. Meteor Atmos Phys 56:81–99

Elsner JB, Kara AB, Owens MA (1999) Fluctuations in north Atlantic hurricane frequency. J Climate 12:427–437

Elsner JB, Jagger TH, Niu X (2000) Shifts in the rates of major hurricane activity over the North Atlantic during the 20th century. Geophys Res Lett 27:1743–1746

Elsner JB, Tsonis AA, Jagger TH (2006) High-frequency variability in hurricane power dissipation and its relationship to global temperature. Bull Amer Met Soc 87:763–768

Emanuel KA (2005) Increasing destructiveness of tropical cyclones over the past 30 years. Nature 436:686–688

Ferreira RN, Schubert WH, Hack JJ (1996) Dynamical aspects of twin tropical cyclones associated with the Madden-Julian Oscillation. J Atmos Sci 53:929–945

Fiorino M, Elsberry RL (1989) Some Aspects of Vortex Structure Related to Tropical Cyclone Motion. J Atmos Sci 46:975–990

Frank WM, Ritchie EA (2001) Effects of Vertical Wind Shear on Hurricane Intensity and Structure. Mon Weather Rev 129:2249–2269

Franklin JL, McAdie CJ, Lawrence MB (2003) Trends in Track Forecasting for Tropical Cyclones Threatening the United States, 1970–2001. Bull Amer Meteor Soc 84:1197–1203

Goerss JS (2000) Tropical cyclone track forecasts using an ensemble of dynamical models. Mon Weather Rev 129:1187–1193

Halverson J, Heymsfield GM, Simpson J, Pierce H, Hock T, Ritchie EA (2006) Warm core structure of Hurricane Erin diagnosed from high altitude dropsondes during CAMEX-4. J Atmos Sci 63:309–324

Hawkins HF, Imbembo SM (1976) The structure of a small, intense hurricane Inez 1966. Mon Weather Rev 104:418–442

Hebert PJ (1980) Atlantic Hurricane Season of 1979. Mon Weather Rev 108:973–990

Jones SC (1995) The evolution of vortices in vertical shear. Part I: Initially barotropic vortices. Quart J Roy Meteor Soc 121:821–851

Jury MR, Enfield DB (2010) Environmental patterns associated with active and inactive Caribbean hurricane seasons. J Climate 23 (8):2146–2160

Jury MR, Santiago MJ (2010) Composite analysis of dust impacts on African easterly waves in the MODIS era. J Geophys Res Atmos. doi:10.1029/2009JD013612

Jury MR, Winter A, Malmgren B (2007) Sub-regional precipitation climate of the Caribbean and relationships with ENSO and NAO. J Geophys Res 112:D16107. doi:10.1029/2006JD007541

Kimball SK, Mulekar MS (2004) A 15-Year Climatology of North Atlantic Tropical Cyclones. Part I: Size Parameters. J Climate 17:3555–3575

Knaff JA, Kossin JP, DeMaria M (2003) Annular Hurricanes. Weather Forecasting 18:204–223

Kruizinga S, Murphy AH (1983) Use of an analog procedure to formulate objective temperature forecasts in Netherlands. Mon Weather Rev 111:2244–2254

Landsea CW (1993) A Climatology of Intense Atlantic Hurricanes. Mon Weather Rev 121:1703–1713

Landsea CW et al (2004) The Atlantic (hurricane) database re-analysis project: documentation for the 1851–1910 alterations and additions to HURDAT. In: Murnane RJ, Liu K-B (eds) Hurricanes and Typhoons: Past, Present and Future. University Press, Columbia, p 464

Maloney ED, Hartman DL (2000) Modulation of hurricane activity in the Gulf of Mexico by the Madden-Julian oscillation. Science 287:2002–2004

McAdie CJ, Lawrence MB (2000) Improvements in tropical cyclone track forecasting in the Atlantic basin, 1970–98. Bull Amer Meteor Soc 81:989–997

McBride JL, Zehr RM (1981) Observational analysis of tropical cyclone formation. Part II: Comparison of nondeveloping vs. developing systems. J Atmos Sci 38:1132–1151

Pasch RJ, Avila LA (1999) Atlantic Hurricane Season of 1996. Mon Weather Rev 127:581–610

Pasch RJ, Avila LA, Guiney JL (2001) Atlantic Hurricane Season of 1998. Mon Weather Rev 129:3085–3123

Pfeffer RL, Challa M (1992) The role of environmental asymmetries in Atlantic hurricane formation. J Atmos Sci 49:1051–1059

Powell MD, Aberson SD (2001) Accuracy of United States tropical cyclone landfall forecasts in the Atlantic basin, 1976–2000. Bull Amer Meteor Soc 82:2749–2767

Root BP, Knight G, Young SG (2007) A fingerprinting technique for major weather events. J Appl Met Clim 46:1053–1066

Sampson CR, Schrader AJ (2000) The Automated Tropical Cyclone Forecast system (v3.2). Bull Amer Meteor Soc 81:1231–1240

Tuleya RE, Kurihara Y (1981) A numerical study on the effects of environmental flow on tropical cyclone genesis. Mon Weather Rev 109:2487–2506

Van den Dool HM (1994) Searching for analogues, how long must one wait? Tellus 46A:314–324

Vislocky RL, Young GS (1989) The use of perfect prog forecasts to improve model output statistical forecasts of precipitation. Wea Forecasting 4:202–209

Webster PJ, Holland GJ, Curry JA, Chang H-R (2005) Changes in tropical cyclone number, duration, and intensity in a warming environment. Science 309:1844–1846

Wong MLM, Chan JCL (2004) Tropical Cyclone Intensity in Vertical Wind Shear. J Atmos Sci 61:1859–1876